Journal of Aerosol Science 54 (2012) 1–12

Contents lists available at SciVerse ScienceDirect

Journal of Aerosol Science

journal homepage: www.elsevier.com/locate/jaerosci

# Electrostatic spray-deposited $CuInGaSe_2$ nanoparticles: Effects of precursors' Ohnesorge number, substrate temperature, and flowrate on thin film characteristics

Ji Hoon Woo [a], Hyun Yoon [a], Ji Hyun Cha [b], Duk Young Jung [b], Sam S. Yoon [a,*]

[a] School of Mechanical Engineering, Korea University Anam-Dong, Seongbuk-Gu, Seoul, 136-713, Republic of Korea
[b] Department of Chemistry, BK-21 School of Molecular Sciences and SKKU Advanced Institute of Nanotechnology, Sungkyunkwan University, Suwon 440-746, South Korea

ARTICLE INFO

*Article history:*
Received 21 December 2011
Received in revised form
7 June 2012
Accepted 7 June 2012
Available online 20 June 2012

*Keywords:*
Nanoparticle
Electrostatic spray deposition
CIGS thin film
Viscosity
Substrate temperature

ABSTRACT

The effect of precursor viscosity, substrate temperature, and flow rate on $CuInGaSe_2$ nanoparticle-based thin films deposited by an electrostatic spray deposition (ESD) technique are studied. ESD is superior to pneumatic spraying because it produces nano-scale, self-dispersive (non-agglomerating), highly wettable (electrowetting) and adhesive droplets, which collectively yield a uniform coating on the substrate. The synthesized $CuInGaSe_2$ nanoparticles were added to 4 different solvents: ethanol (E), butyl carbitol (BC), ethylene glycol (EG), and diethylene glycol (DEG). Subsequently, the solvents were electrostatically sprayed onto a molybdenum-coated soda-lime glass substrate. The solvent that yielded the most uniform surface morphology for the coated materials was identified. The surface roughness of the coated CIGS thin film, which depends on viscosity and the substrate temperature, was studied by AFM characterization.



## 1. Introduction

Copper indium selenide (CIS)-based thin films are the most promising candidates to improve cost competitiveness among common thin-film solar cells (e.g., amorphous silicon (a-Si), cadmium telluride (CdTe), gallium arsenide (GaAs), CIS, or CuIn(Ga)Se). CIS-based solar cells are attractive because they: (1) minimize material consumption, (2) provide low-cost substrates (e.g., soda-lime glass, stainless steel, foil, and polymers), (3) are flexible, light, strong, and thin substrates that are resistant to degradation caused by solar radiation and severe environments, (4) have favorable optical and electrical properties such as tunable band gaps from 1 to 2.4 eV through addition of gallium (Ga) and sulfur (S) that capture shorter wavelength light, (5) have large photon absorption coefficients, and (6) have high power-conversion efficiencies of 15–20%. However, advances in CIS-based solar cells have been hampered by high manufacturing costs and the capital and energy requirements of conventional vacuum deposition methods (e.g., co-evaporation and sputtering). Non-vacuum-based deposition methods would greatly reduce costs and enhance solar-energy-technology market penetration.

Non-vacuum methods include spin-coating, electro-deposition, screen-printing, doctor-blading, paste coating, print precursor, and spray pyrolysis (Mitzi et al., 2008). We are particularly interested in spray pyrolysis because of (1) its ability to cover large areas, (2) simultaneous process of spraying and heat addition (i.e., pyrolysis via substrate heating), (3) the

* Corresponding author.
*E-mail address:* skyoon@korea.ac.kr (S.S. Yoon).

0021-8502/$ - see front matter © 2012 Elsevier Ltd. All rights reserved.
http://dx.doi.org/10.1016/j.jaerosci.2012.06.003

option of using either solution- or particle-based precursors, and (4) its use of low viscosity solvents (other non-vacuum methods, such as doctor-blading or paste-coating, require highly viscous solvents to prevent dripping). Also, high viscosity solvents contain impurities (i.e., Cl, O, C, N, and Na) that add resistance and degrade solar cell performance.

Solution-based precursors typically involve the dissolution of salts (i.e., $CuCl_2$, $Cu(NO_3)_2$, $InCl_3$, $Ga(NO_3)_3$, *N*-dimethyl selenourea, or thiourea), which are completely ionized in water or an alcohol-based solvent. If these dissolved salts are electro-sprayed, exceedingly small drops are produced via Rayleigh explosion or fission. This fission process facilitates uniform coating. Furthermore, solution-based approaches exhibit low toxicity (as long as selenium is not used during spraying; selenium can be incorporated during a post-selenization process). However, the efficiency of solar cells produced with this solution-based approach has historically been low; Tomar and Garcia (1982) demonstrated a 2% conversion efficiency with a spray-coated thin film solar cell of ZnO/$CuInSe_2$. Ahn et al. (2010) reported a 2% conversion efficiency for their solar cell produced by doctor-blading. Yoon et al. (2011) reported a 1.78% conversion efficiency with an electrostatically spray-deposited $CuInSe_2$ film with a conventional Mo/CIS/CdS/*i*-ZnO/*n*-ZnO/Al structure.

Compared to solution-based approaches, making and handling CIGS nanoparticles add additional expenses. However, particle-based approaches may still be worthwhile because of their conversion efficiencies. Norsworthy et al. (2000) reported a conversion efficiency of 10.5% for their CIS film. They used Cu-In metallic powders with mean particle size less than a micron. They spray deposited a Cu–In alloy, which was dispersed in water mixed with a wetting agent and a dispersant. Eberspacher et al. (2001) achieved a conversion efficiency of 11.7% by mitigating layer porosity when depositing CIS nanoparticles. Kapur et al. (2003) reported a 13.5% conversion efficiency for their CIGS solar cells.

Despite the high efficiencies of nanoparticle approaches, issues still remain. When using sprays to deliver nanoparticles onto a substrate, particle dispersion is a critical issue. Particle agglomeration greatly depends on the thermo-physical properties of the carrying solvent. For example, if the solvent viscosity is not appropriate, then nanoparticles can agglomerate, effectively eliminating their nano size. Therefore, we investigated the effect of solvent viscosity on dispersion of CIGS-nanoparticles as deposited onto a substrate by electrostatic spray. The solvent that yielded the most uniform surface morphology for the coated materials was identified by scanning electron microscopy (SEM) and atomic force microscopy (AFM). The surface roughness of the coated CIGS thin film, which depended on viscosity and the substrate temperature, was also reported both quantitatively and qualitatively.

## 2. Experimental setup

### 2.1. CIGS particle synthesis

High-purity ternary and quaternary $CuIn_xGa_{1-x}S_2$ nanoparticles were synthesized with a sonochemical process under ambient conditions. Sonochemical techniques have often been used to generate nanosized particles (small particles with high specific surface area) (Zhu et al., 1999; Lee et al., 2011). The indium to gallium ratio and the size of the particle was controlled by varying the reaction conditions. Our CIGS nanocrystals are about 3 nm according to the Scherrer equation, which uses XRD peaks to estimate the crystallite size. The broader the width of the peaks, the smaller the crystallite size; they are inversely proportional. Thus It should be noted that, because of complexities in the material composition, it is possible that minor deviations in the composition leading to minor variations of the lattice constant may lead to an error in estimation of the particle size. This initial particle size will significantly increase by two to three orders of magnitudes after they are mixed with solvents.

CuCl (0.6 mol), an indium acetate—$In(OAc)_3$ (0.42 mol), $Ga(NO_3)_3 \cdot xH_2O$ (0.18 mol), and Se powder (1.2 mol) were mixed with ethylene glycol and hydrazine monohydrate (98%). (Warning: hydrazine monohydrate is highly toxic and may be fatal if inhaled, swallowed, or absorbed through the skin and must be handled with personal protective equipments to prevent contact). The mixture was stirred with a high-power ultrasonic generator (Hielscher Ultrasonic GmbH) for 3 h under ambient pressure conditions at 110 °C. The product was centrifuged and washed with degassed water several times and dried at room temperature for further characterization. The final CIGS particles are shown in Fig. 1.

### 2.2. Precursor preparation

Four different precursors were prepared by mixing the CIGS nanoparticles with four different working solvents; pure ethanol (E), butyl-carbitol (BC), ethylene glycol (EG), and diethylene glycol (DEG), listed in the order of increasing viscosity and density. Variations in surface tension and density were less than the variations of viscosity. Physico-chemical properties of the solvents are listed in Table 1. No surfactant was added to any of the precursors. Butyl-carbitol provided a good balance of volatility, solvency, water solubility, and jet stability because of its relatively high viscosity and surface tension. Alternatively, butyl carbitol exhibited the highest molecular weight and thus its impurity content was expected to be the highest. Ethanol was expected to yield the lowest impurity content because of its low carbon and oxygen content. In addition, ethanol had the lowest boiling point, which in turn facilitated evaporation of the solvent at relatively low substrate temperatures. Impurity content can be minimized by evaporating as much of the solvent as possible. A coated film should be thin enough so that much of the deposited solvent can readily evaporated before closure of the top surface during the crystallization process (i.e., pyrolysis or/and selenization). Another solvent such as 1,2-propanediol could have been investigated; however, it was previously reported that 1,2-propanediol promoted nanoparticle agglomeration and its

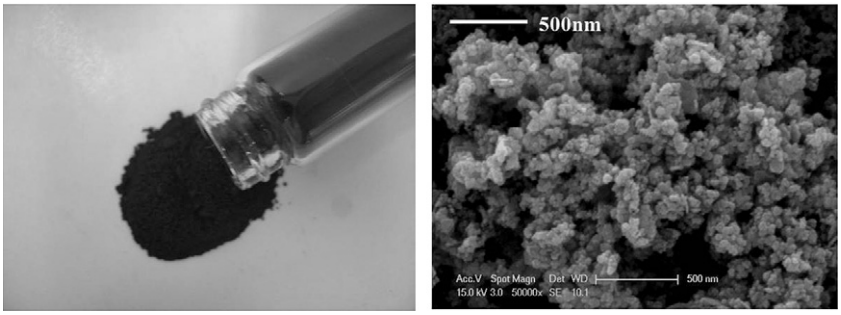


**Fig. 1.** CIGS nanoparticles and its SEM image. The raw powder in the left image comprises particles of $1–10^1$ nm. After mixing them with solvents, the agglomerated particles reach the size of $10^2–10^3$ nm.

**Table 1**
Physico-chemical properties of the solvents.

| Fluid | Ethyl alcohol $C_2H_5OH$ | Butyl carbitol $C_4H_9(OCH_2CH2)_2OH$ | Ethylene glycol $C_2H_6O_2$ | Diethylene glycol $C_4H_{10}O_3$ |
|---|---|---|---|---|
| Molecular weight [g/mol] | 46.07 | 162.23 | 62.07 | 106.12 |
| $\rho$, Density [kg/m$^3$] | 789 | 955 | 1109 | 1110 |
| $\sigma$, Surface tension [mN/m] | 22.1 | 30 | 47.7 | 44.8 |
| $\mu$, Viscosity [cP] | 1.2 | 5.17 | 16.1 | 30 |
| Boiling point [°C] | 78 | 231 | 197 | 245 |

dispersivity was worse than ethanol (Kaelin et al., 2004). All precursors were ball-milled for 72 h, after which they were immediately sprayed onto substrates. All preparations were formulated at room temperature in air.

### 2.3. Electrostatic spray deposition system

Electrostatic spray deposition (ESD) is used in this study. ESD is superior to the conventional pneumatic spraying method because it produces extremely fine (sub-micron), self-dispersive (non-agglomerating), highly wettable (electro-wetting), and adhesive drops to yield a uniform coating on the substrate (Jaworek and Sobczyk, 2008) as shown in Fig. 2(a). In addition, because charged drops were accelerated toward the substrate, targeting was improved, which resulted in high deposition efficiency. Several researchers have produced thin films for solar applications using ESD (Fujimoto et al., 2006; Roncallo et al., 2008, 2011). Kaelin et al. (2004) suspended 100-nm Cu–In nanoparticles in ethanol and 1,2-propanediol carriers to apply a thin film that was subsequently augmented with a selenization process to make a CIS film. They concluded that ESD provided improved surface morphology over the doctor-blading and the screen-printing techniques. ESD $TiO_2$-based solar cells have been extensively studied by Hogan and Biswas (2008) and Modesto-Lopez and Biswas (2010).

The ESD system setup is shown in Fig. 2(b). The downward-facing nozzle center was aligned with the plate center separated by a 45-mm gap with a variable cone angle depending upon the flowrate. The substrate material was a $25 \times 25$-mm$^2$ molybdenum-coated soda-lime glass. The precursor dispenses from a syringe pump with flowrate adjusted to yield a stable Taylor cone-jet, which produced the smallest drops possible under the given operating conditions. The nozzle inner diameter was 3 mm. A voltage-supply wire was attached to the charging needle (i.e., anode) and the substrate was grounded (i.e., cathode). Typically, a CIGS film of about 1-μm thickness developed in less than 4 min. Precursor flowrates range from 0.1 to 1.6 mL/h under applied voltages of 1–20 kV, yielding droplet sizes around a few 100 nm. The process parameters used during the thin film deposition are listed in Table 2.

### 2.4. Substrate characteristics

While spraying CIGS nanoparticles, the Mo-coated substrate temperature was maintained within a temperature range of $60-340$ °C to facilitate precursor evaporation (and some degree of pyrolysis) and to form a solid thin film; see Table 3. Molybdenum substrates provide the best back-contact (or electrode) performance because of their superior electrical conductivity and interfacial adhesion between the CIGS absorber layer and the electrode (Dhere and Dhere, 2005). Indium tin oxide (ITO) or fluorine tin oxide (FTO) substrates have been used as substitutes; however, they have shown poorer performance for CIGS solar cells (Romeo et al., 2004) in comparison to Mo-coated substrates. Furthermore, ITO and FTO do not withstand the high-temperature requirements of the post-annealing or selenization process.

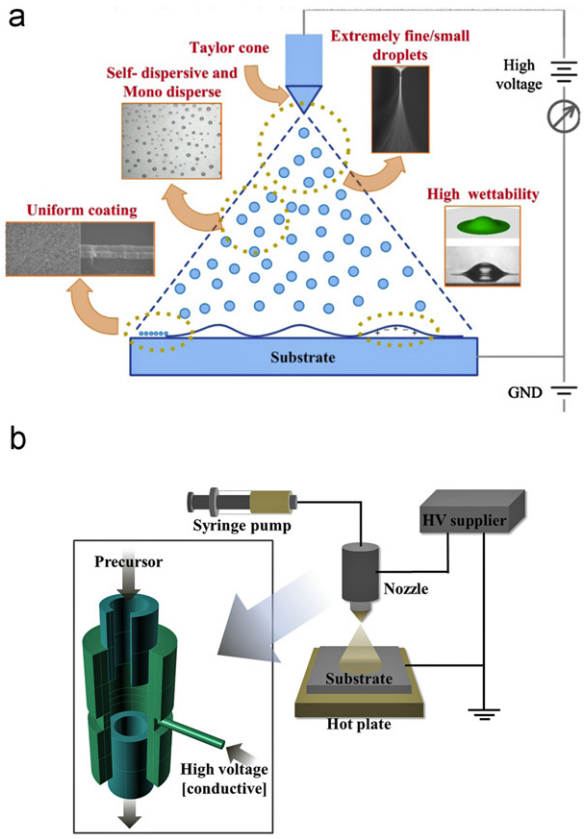


**Fig. 2.** (a) Advantages of the ESD (electrostatic spray deposition) system and (b) schematic of the experimental setup.

**Table 2**
Process parameters for the ESD system.

| Solvent | Flowrate $Q$ [mL/h] | Voltage $V$ [kV] | Nozzle diameter $d_n$ [mm] | Separation distance [mm] | Substrate temperature [°C] |
|---|---|---|---|---|---|
| Ethanol | 0.4 | 6–8 | 3 | 40 | 62.4–94 |
| Butyl-carbitol | | 8–17 | | | 130–332 |
| Ethylene-glycol | | 10–19 | | | 158–236 |
| Diethylene-glycol | | 10–20 | | | 196–294 |

*Note*: The nozzle diameter ($d_n$) is 3 mm and the corresponding injection speed is $U=1.57\times10^{-5}$ m/s for $Q=0.4$ mL/h.

**Table 3**
Substrate temperatures.

| Fluids | Substrate temperature (°C) | | |
|---|---|---|---|
| | 80% BP | 100% BP | 120% BP |
| Ethanol | 62.4 | 78 | 94 |
| Butyl carbitol | 130 | 231 | 332 |
| Ethylene glycol | 158 | 197 | 236 |
| Diethylene glycol | 196 | 245 | 294 |

## 3. Results and discussion

### 3.1. Effects of viscosity

Thin films (about 1 μm thickness is most suitable) minimize cost and allow efficient evaporation of the carrying solvent for non-vacuum-based spray-coated applications. If the film is too thick (i.e., greater than 3 μm), only the top part of the

film gets crystallized (or selenized) and the layer between the crystallized surface and the Mo-substrate remains porous and contains trapped impurities from the incompletely evaporated solvent (Norsworthy et al., 2000). The use of an electrostatic spray is suitable for thin films because it generates nano-scale drops. The smaller the drop size, the thinner the film. However, even ESD CIGS nanoparticles can aggregate regardless of the solvent's viscosity. If the nanoparticles are poorly dispersed in the precursor, CIGS nanoparticles aggregate and yield inappropriately large particles and hinder development of a uniform coating.

In general, viscosity slows the aggregation process by either promoting a proton-exchange mechanism that opposes sedimentation (Hughes et al., 1999), or by increasing the surface potential that increases the particle inter-repulsion. The solvents listed in Table 1 were selected to have widely varying viscosities to facilitate study of CIGS nanoparticle aggregation. Table 4 lists the Reynolds (*Re*), Weber (*We*), and Ohnesorge (*Oh*) numbers for all of the solvents used in the current studies. The Ohnesorge number is 0.005 for E, increases monotonically through BC and EG and is largest for DEG at 0.8.

After ball milling, precursors were immediately sprayed for 4 min at a volume flowrate of 0.4 mL/h onto the Mo substrate; the total volume of the sprayed solvent was $V_s = 2.67 \times 10^{-8}$ m$^3$. The deposited thin film volume was $V_t = 25 \times 25 \times 1$ μm$= 6.25 \times 10^{-8}$ m$^3$. By carefully measuring volumes occupied by particles and dried solvents based on SEM images (both side and top views), the thin-film volume comprising CIGS particles is $\alpha \approx 90\%$ with the remaining 10% as dried solvent. Given that the ratio of the particle volume to the solvent volume was $\beta = 10\%$, the deposition efficiency is calculated as $\eta_d$=(Deposited particle volume)/(Sprayed particle volume)$=(\alpha \times V_t)/(\beta \times V_s) = 21\%$. Moderate pyrolysis was expected during the deposition process because the substrate was maintained near the solvent's boiling point. Significant additional pyrolysis will occur during the selenization process, which takes place at a temperature much higher than the solvent's boiling point ($T_{bp}$). The substrate temperature was varied from 80% to 120% of the solvent's boiling point. Substrate temperatures lower than 80% of the solvent's boiling point yielded excessive wetting and even precursor dripping.

Figs. 3–6 show side (top row) and top (bottom row) SEM images of CIGS particles coated onto the Mo-substrates when using E, BC, EG, and DEG, respectively. The images from the first, second, and third columns correspond to the results obtained at substrate temperatures of 80%, 100%, and 120% of each solvent's boiling point, respectively.

Significant aggregation was observed for E, as shown in Fig. 3. Because of these large aggregated particles, the Mo-substrate was not entirely covered; E was not considered further as a candidate solvent for the selenization process. Fig. 4 shows that the BC film was better than E, but aggregation was also observed in BC reservoir after 5 min of spraying and it was not be considered further, especially for longer spray durations. The EG solvent in Fig. 5 exhibited coronal discharge because its high conductivity hindered stable spraying of the precursor (Sastry & Reddy, 1983; Jackson et al., 1987; Parretta et al., 1998). DEG films in Fig. 6 seem to be the best among the precursor candidates as they yielded the smallest particle sizes and most uniform thin films at all temperatures.

**Table 4**
Precursors Reynolds and Weber numbers defined as $Re = \rho U d_n/\mu$, $We = \rho U d_n^2/\sigma$, where $U = Q/A$, $A = \pi d_n^2/4$, and $d_n = 3$ mm. The flowrate is fixed at $Q = 0.4$ mL/h.

| Precursor solvent | $Re \times 10^3$ | $We \times 10^8$ | $Oh = (We)^{1/2}/Re$ |
|---|---|---|---|
| Ethanol | 31.01 | 2.65 | 0.0053 |
| Butyl carbitol | 8.71 | 2.36 | 0.0177 |
| Ethylene glycol | 3.25 | 1.723 | 0.0404 |
| Diethylene glycol | 0.17 | 1.837 | 0.7980 |

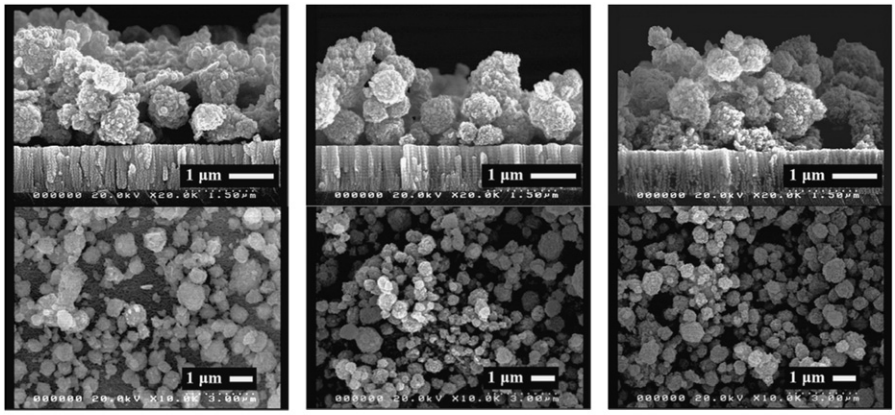


**Fig. 3.** SEM micrographs of an ESD CIGS thin film from an E solvent on a Mo substrate at various temperatures.

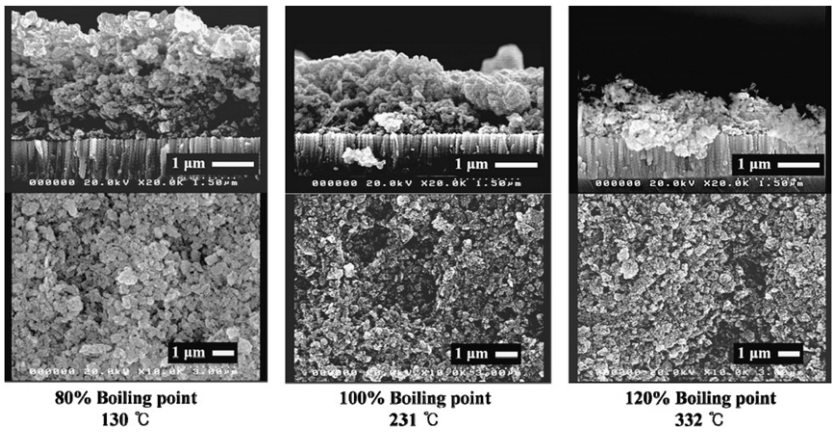


**Fig. 4.** SEM micrographs of an ESD CIGS thin film from a BC solvent on a Mo substrate at various temperatures.

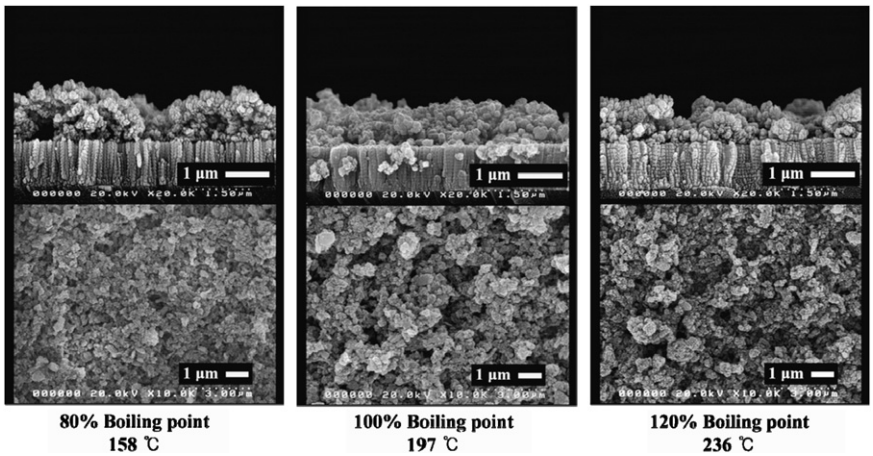


**Fig. 5.** SEM micrographs of an ESD CIGS thin film from an EG solvent on a Mo substrate at various temperatures.

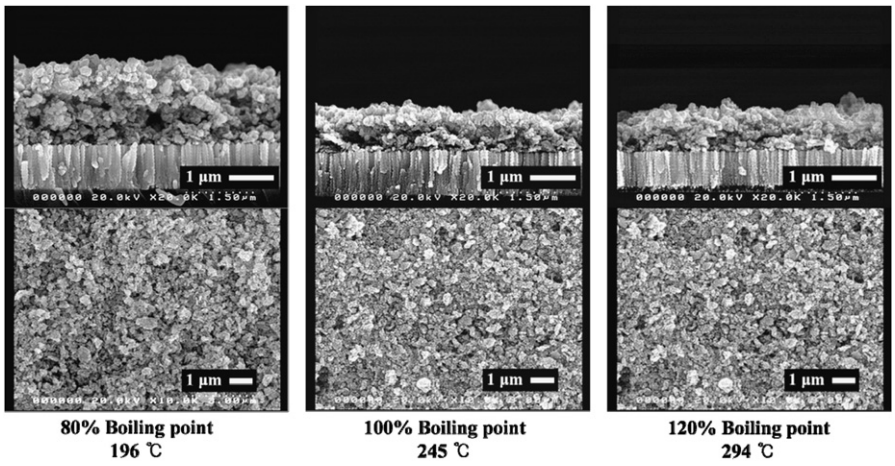


**Fig. 6.** SEM micrographs of an ESD CIGS thin film from a DEG solvent on a Mo substrate at various temperatures.

Fig. 7 shows the maximum and minimum size of the CIGS particles in conjunction with Figs. 3–6 for substrate temperatures at 80% of the solvent's boiling temperature as a function of the Ohnesorge number ($Oh=\mu/(\rho\sigma d_n)^{0.5}$), which is the measure of the viscosity effects; the higher the *Oh*, the stronger the viscosity effect. The solid and dashed-lines are the linear fits for the experimental data at maximum and minimum particle size, respectively. The trend shown in Fig. 7 is indicative of the degree of

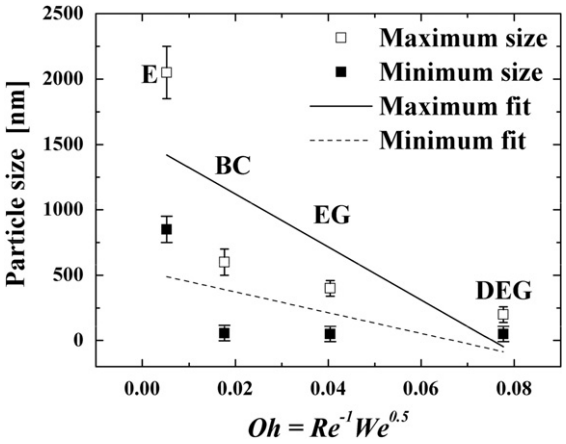


**Fig. 7.** Effects of Ohnesorge number on minimum and maximum sizes of CIGS particles from ESD with substrate temperatures at 80% of the solvent boiling points.

aggregation. The E precursor exhibited the largest particle size and the DEG precursor the smallest; particle size decreased with increasing viscosity. The particle size was estimated by counting pixel numbers of the SEM images. A total of 30–40 particles were randomly selected per SEM image and the sizes reported in Fig. 7 are the arithmetic means.

### 3.2. Effect of substrate temperature

Viscosity was not the only parameter affecting thin and uniform CIGS films; the substrate temperature also showed a discernable effect on the film quality (though not as significant as viscosity). At high substrate temperatures (i.e., higher than the boiling point of the solvent), drops tended to evaporate before reaching the substrate, and therefore many of the particles deposited onto the substrate were already dried. Voids or gaps among particles were prevalent and porosity became an issue for high substrate temperatures. Furthermore, buoyancy-driven hot air destabilized the cone-jet, thereby decreasing ESD coating efficiency.

At low substrate temperatures, the coating process required increased time for the solvent to evaporate. Excessive wetting may result and precursor dripping observed occasionally. An optimal substrate temperature minimizes both issues (excessive wetting and elevated porosity). This optimal substrate temperature is high enough to initiate the drop evaporation process and also low enough to receive drops in the liquid phase so that they wet the existing layer and fill gaps and voids among particles; this yields a dense film.

Figs. 3–6 show the effect of substrate temperature (i.e., 80%, 100%, and 120% of $T_{bp}$) on thin films. For E in Fig. 3, determining whether substrate temperature has any effect on the thin-film morphology was difficult because particle aggregation was the dominant factor. For BC in Fig. 4, increasing the substrate temperature increased the rate of evaporation and generated a thinner film. Also, particle size was reduced at higher substrate temperatures. For EG in Fig. 5, there was no discernable effect of substrate temperature on the thickness of the film; however, increased substrate temperature tended to yield larger particles. For DEG in Fig. 6, a thinner film was formed when substrate temperature was high, but there was no discernable effect on particle size.

As mentioned previously, Fig. 7 shows the variation of maximum and minimum particle sizes as a function of the Ohnesorge number (i.e., $Oh = Re^a We^b$, where $a = -1$ and $b = 0.5$) at 80% of the solvent boiling point. At a higher substrate temperature (i.e., 120% of $T_{bp}$), the variation of particle size with $Oh$ is shown in Fig. 8(a) at 120% $T_{bp}$. Because it is still desirable to delineate the particle size trend for 120% of $T_{bp}$ substrate temperature, we have adopted a model similar to the Ohnesorge number using $K = Re^a We^b$. A linear fit to the data using $a = 0.04$ and $b = -0.14$ is shown in Fig. 8(b). The fit allows the average particle size ($D_p$) to be cast as a function of $K$; $D_p = 3020\ K - 28314$ for the maximum particle size and $D_p = 1305\ K - 12366$ for the minimum particle size, where $K = \sigma^{0.14}/(\mu^{0.04}\rho^{0.1}U^{0.24}d_n^{0.1})$.

Fig. 9 shows AFM images of thin films coated with various solvent-based CIGS precursor at different substrate temperatures. These images were plotted on the same length scale to facilitate direct comparison. The DEG surface was most uniform at all temperatures. The second best uniformity was seen for BC and the worst uniformity for E. Quantitative data from the images of Fig. 9 are shown in Fig. 10, where the average surface roughness is plotted as a function of substrate temperature; increasing substrate temperature roughened the surface of the thin film. At high substrate temperatures, the Leidenfrost effect may occur (Choy & Su, 2001), where a thin vapor layer around a depositing drop inhibits deposition. At even higher substrate temperatures, sprayed drops completely evaporated prior to deposition; dried agglomerates were deposited. Evaporation of the spray and dried aggregate deposition is the likely reason for the roughened surfaces at higher temperatures.

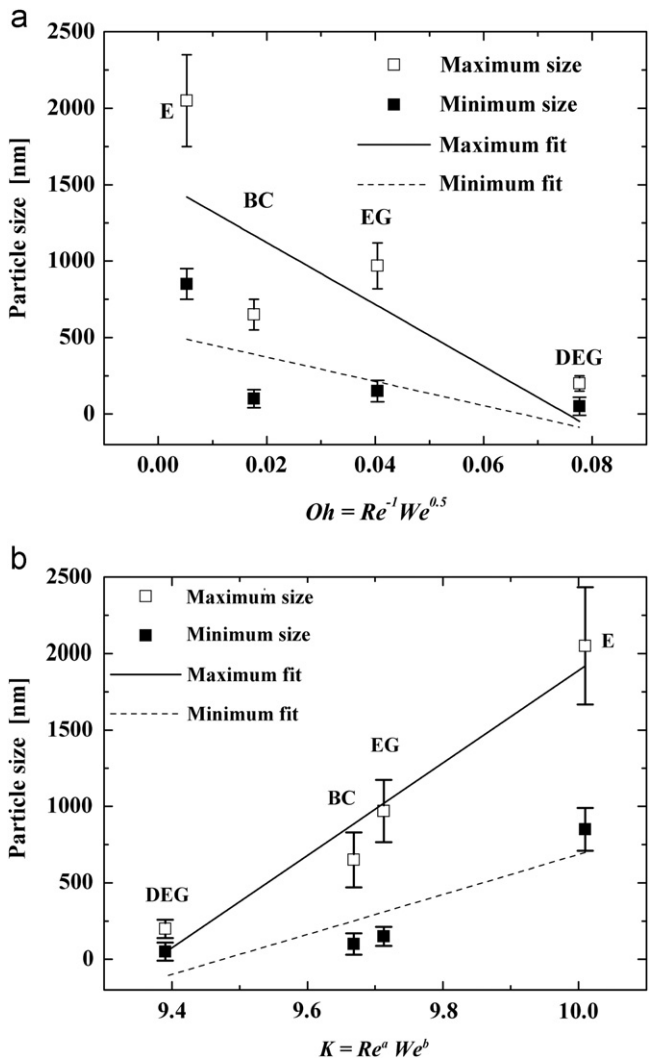


**Fig. 8.** Minimum and maximum sizes of CIGS particles from ESD with substrate temperatures at 120% of the solvent boiling points. (a) The effect of *Oh* and (b) the effect of *K* with constants of $a=0.04$ and $b=-0.14$.

### 3.3. XRD analysis

Fig. 11 shows the thin-film XRD results at various temperatures for E, BC, EG, and DEG precursors. In general, increasing temperature reduced the peak intensity; this was because increased porosity at higher temperatures hindered the formation of highly crystallized dense films. This suggests that lower substrate temperature is better for obtaining dense, highly crystallized films. The broadening and decreased peak intensities are due to the poorly developed crystalline structure of the film. Also, it is worth noting that the peak at 26.6° corresponds to the (1 1 2) planes of a chalcopyrite structure.

The peak intensities of E and EG are higher than those of BC and DEG; better crystalline structure was observed for E and EG. Aggregation was prominent for E and EG and XRD shows that aggregation can improve the crystalline structure. Unfortunately, DEG, which had the least aggregation and best surface uniformity, also had the smallest XRD peaks. Nevertheless, the low XRD peaks may not be an issue because these peaks will be enhanced through the selenization process where polymer impurities will be removed by rapid evaporation as further crystallization takes place.

### 3.4. Effect of flowrate

For electrostatic sprays, the drop size ($d$) is proportional to the square-root of the flowrate ($Q$); $d \propto Q^{1/2}$ (Gañán-Calvo, 1997). If $Q$ decreases, then the drop size becomes smaller and, in theory, one may assume a finer and thinner coating.

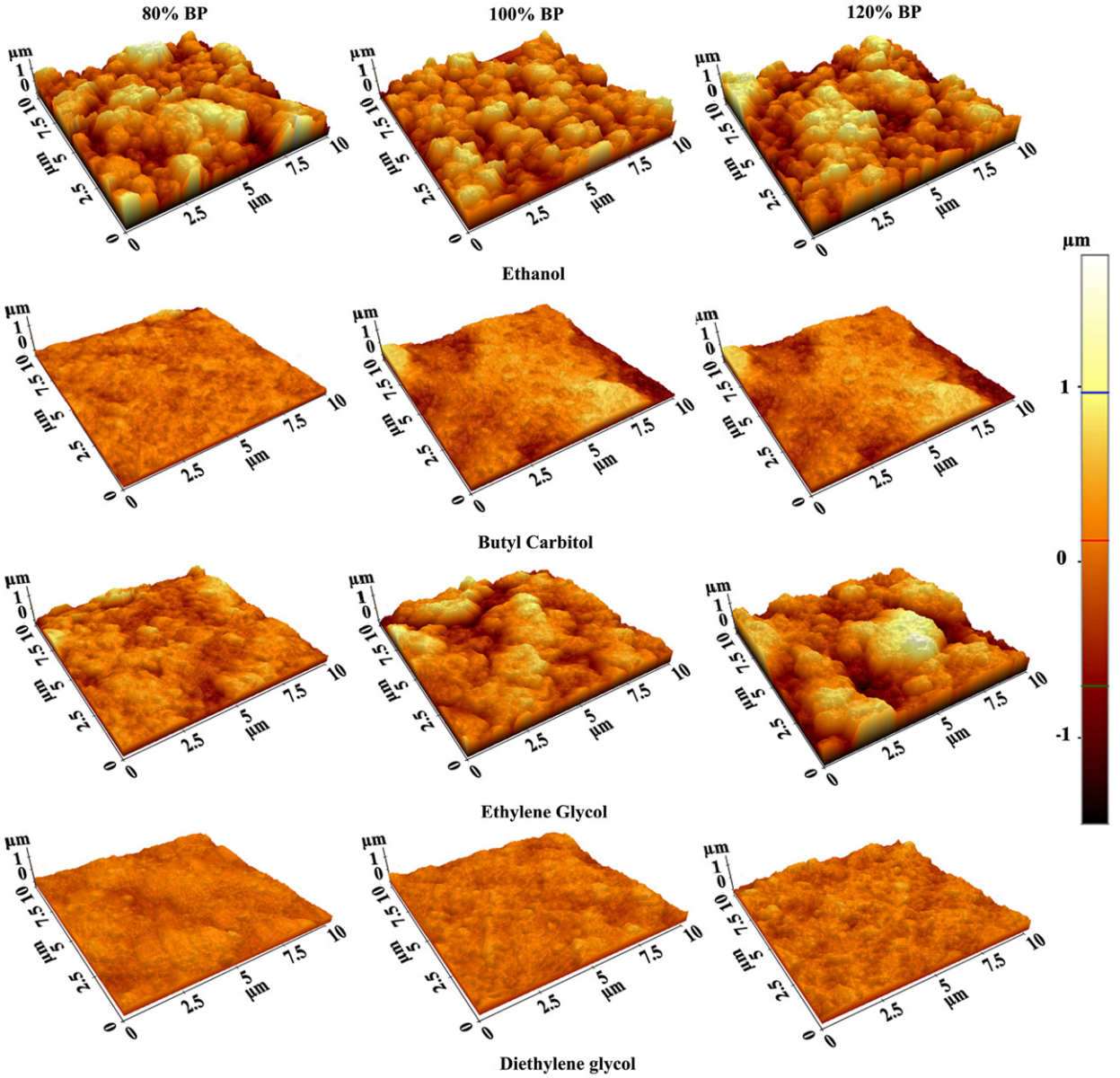


**Fig. 9.** AFM images of thin films from solvents at various substrate temperatures.

However, in reality, there exists an optimal drop size, which should be large enough to preclude pre-contact evaporation but small enough to avoid excessive wetting and yield a dense, low-porosity thin film.

Also, the effect of flowrate on spray coverage area and particle aggregation using DEG was examined. Fig. 12 shows that the average particle size was minimized when the flowrate was 0.4 mL/h, a near optimal flowrate. For flowrates less than 0.4 mL/h, the drop size was too small and drying dominated, resulting in increased film porosity. Dried, agglomerated particles were relatively large, as shown in the pattern in Fig. 12. Conversely, for flowrates greater than 0.4 mL/h, the drop size was too large and wetting dominated. In fact, agglomeration was increased because of the Marangoni effect that drives nanoparticles toward periphery of the evaporating solvent. So, large flow rates also yielded large particles.

Fig. 12 also shows that spray coverage increases with flow rate. To sustain the Taylor cone mode at all flowrates, the applied voltage should be increased when the flowrate is increased. In turn, drop charges increased thereby increasing electrostatic repulsion. Consequently, larger spray coverage areas were observed at larger flowrates. Fig. 13 summarizes the results stated in Section 3.

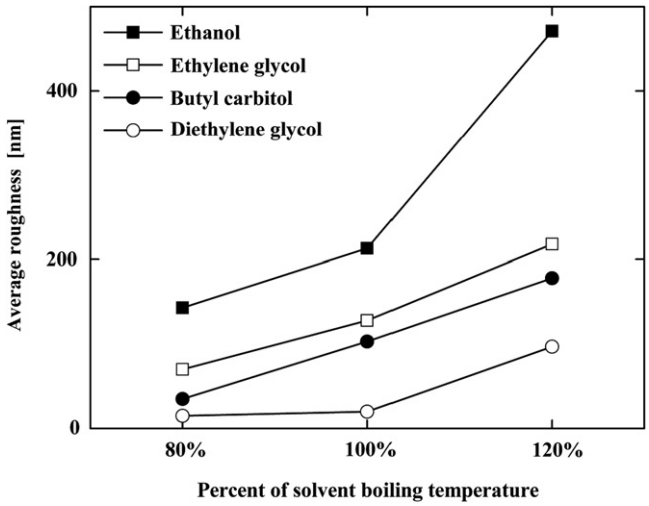


**Fig. 10.** Effect of substrate temperature on average roughness of the thin films.

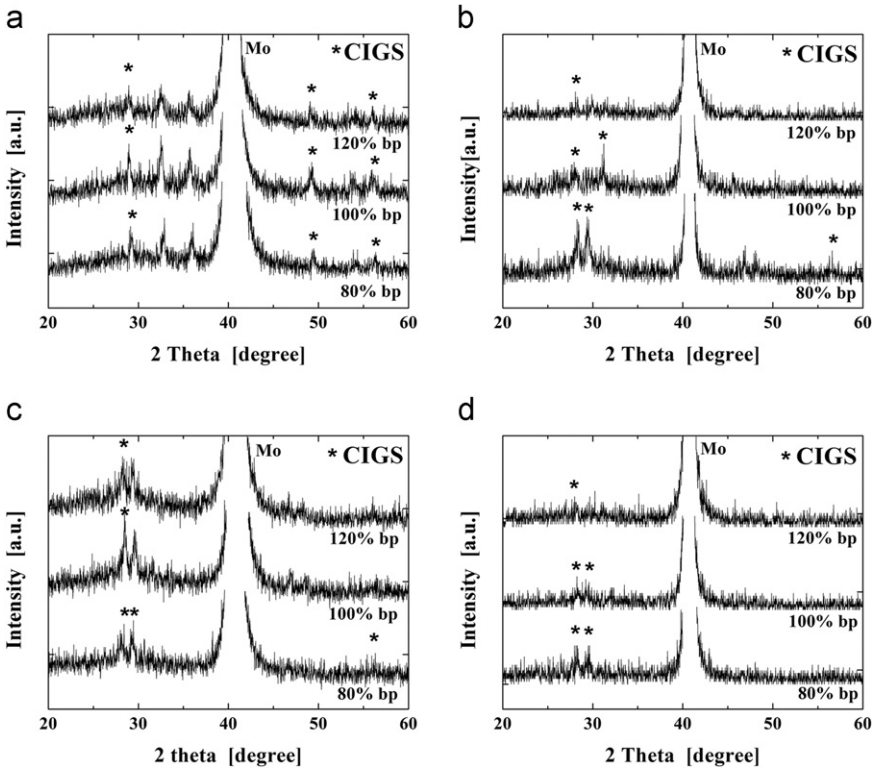


**Fig. 11.** XRD of CIGS nanoparticle-based thin films using 4 different solvents. (a) Ethonal, (b) butyl carbitol, (c) ethylene glaycol and (d) diethylene gycol.

## 4. Conclusion

A non-vacuum-based ESD technique was used to deposit CIGS nanoparticles onto molybdenum-coated glass. ESD produces extremely fine, self-dispersive, highly wettable, and adhesive drops to yield a uniform coating on the substrate. Furthermore, ESD covers large areas and augments crystallization because of heat transfer through the substrate. Because nanoparticle aggregation is problematic, we investigated the effect of solvent viscosity on dispersion of CIGS nanoparticles. Four different precursors were studied: pure ethanol, butyl-carbitol, ethylene glycol, and diethylene glycol. Significant aggregation was observed for ethanol; the Mo-substrate was not entirely covered because of these large aggregated particles. For butyl-carbitol, aggregation was observed after 5 min of spraying and demonstrates that BC should not be

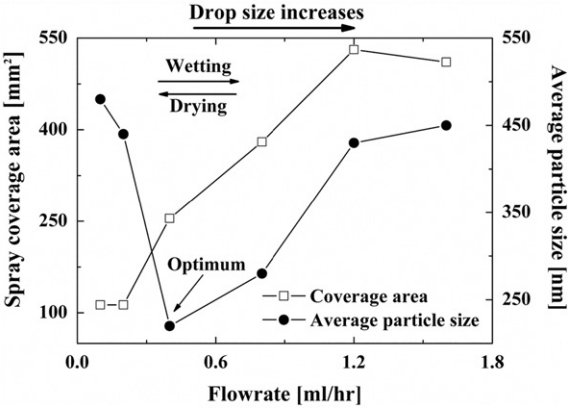


**Fig. 12.** Effect of DEG flowrate on spray coverage area and average particle size.

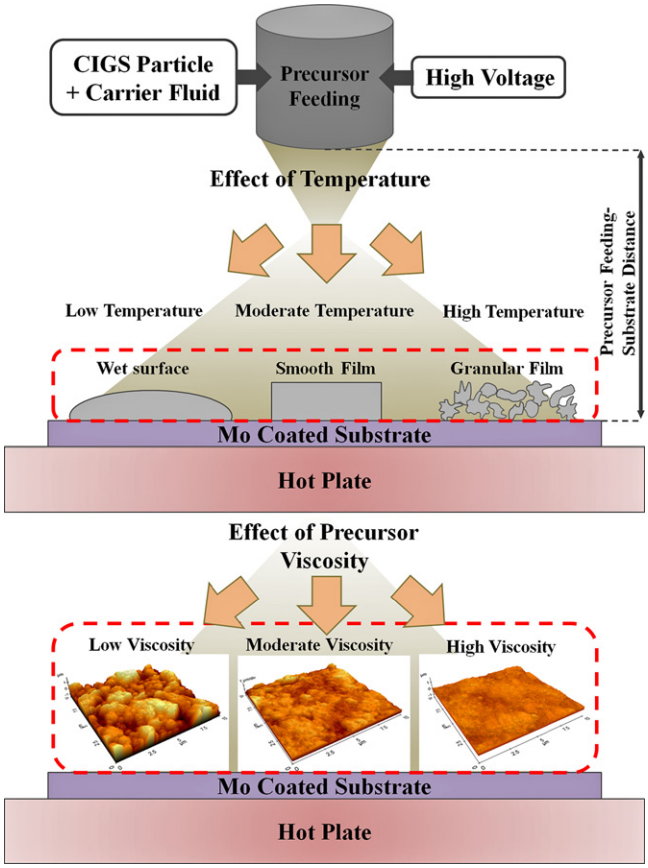


**Fig. 13.** Summary of current studies: the substrate temperature effect and the solvent viscosity effect.

used for lengthy spraying operations. Ethylene glycol yielded coronal discharge due to its high conductivity, which hindered stable spraying of the precursor. The DEG precursor performed best among those studied as it yielded the smallest particles size and most uniform thin film at all substrate temperatures. Its high viscosity is a boon. But at the highest substrate temperature (i.e., higher than the boiling point of the solvent), drops evaporated before they reach the substrate, and therefore only dried particles were deposited onto the substrate. Voids or gaps among particles increased porosity at elevated substrate temperatures. At low substrate temperatures, evaporation was slow and wetting excessive. An optimal substrate temperature minimizes both issues.

## Acknowledgement

This work was supported by the Human Resources Development of the Korea Institute of Energy Technology Evaluation and Planning (KETEP, No. 20104010100640), National Research Foundation of Korea (NRF-2012-0001169), and the Converging Research Center Program through the Ministry of Education, Science and Technology (2010K000969). This work was also supported by the National Research Foundation of Korea (NRF-2011-0030433 and 2010-0010217) grant funded by the Korean government (MEST) and by a grant from the cooperative R&D Program (B551179-08-03-00) funded by the Korea Research Council Industrial Science and Technology.

## References

Ahn, S., Kim, C., Yun, J.H., Gwak, J., Jeong, S., Ryu, B.-H., & Yoon, K. (2010). $CuInSe_2$ (CIS) thin film solar cells by direct coating and selenization of solution precursors. *Journal of Physical Chemistry C*, *114*, 8108–8113.

Choy, K.L., & Su, B. (2001). Growth behavior and microstructure of CdS thin films deposited by an electrostatic spray assisted vapor deposition ESAVD Process. *Thin Solid Films*, *388*, 9–140.

Dhere, N.G., & Dhere, R.G. (2005). Thin-film photovoltaics. *Journal of Vacuum Science and Technology A*, *23*, 1208.

Eberspacher, C., Fredric, C., Pauls, J., & Serra, K. (2001). Thin-film CIS alloy PV materials fabricated using non-vacuum, particles-based techniques. *Thin Solid Films*, *387*, 18–22.

Fujimoto, M., Kado, T., Takashima, W., Kaneto, K., & Hayase, S. (2006). Dye-sensitized solar cells fabricated by electrospray coating using $TiO_2$ nanocrystal dispersion solution. *Journal of the Electrochemical Society*, *153*, A826–A829.

Gañán-Calvo, A.M. (1997). Cone-jet analytical extension of Taylor's electrostatic solution and the asymptotic universal scaling laws in electrospraying. *Physical Review Letters*, *79*, 217–220.

Hogan, C.J., & Biswas, P. (2008). Porous film deposition by electrohydrodynamic atomization of nanoparticle sols. *Aerosol Science and Technology*, *42*, 75–85.

Hughes, D.F.K., Robb, I.D., & Dowding, P.J. (1999). Stability of copper phthalocyanine dispersions in organic media. *Langmuir*, *15*, 5227–5231.

Jackson, S.C., Baron, B.N., Rocheleau, R.E., & Russell, T.W.F. (1987). A chemical reaction model for physical vapor deposition of compound semiconductor films. *AICHE Journal*, *33*, 711–721.

Jaworek, A., & Sobczyk, A.T. (2008). Electrospraying route to nanotechnology: an overview. *Journal of Electrostatics*, *66*, 197–219.

Kaelin, M., Zogg, H., Tiwari, A.N., Wilhelm, O., Pratsinis, S.E., Meyer, T., & Meyer, A. (2004). Electrosprayed and selenized Cu/In metal particle films. *Thin Solid Films*, *457*, 391–396.

Kapur, V.K., Bansal, A., Le, P., & Asensio, O.I. (2003). Non-vacuum processing of $CuIn_{1-x}Ga_xSe_2$ solar cells on rigid and flexible substrates using nanoparticle precursor inks. *Thin Solid Films*, *431–432*, 53–57.

Lee, J.H., Chang, J., Cha, J.-H., Lee, Y., Han, J.E., Jung, D.-Y., Choi, E.C., & Hong, B. (2011). Large-scale, surfactant-free solution syntheses of $Cu(In,Ga)(S,Se)_2$ nanocrystals for thin film solar cells. European Journal of Inorganic Chemistryn/a-n/a.

Mitzi, D., Yuan, M., Liu, W., Kellock, A., Chey, S., Deline, V., & Schrott, A. (2008). A high-efficiency solution-deposited thin-film photovoltaic device. *Advanced Materials*, *20*, 3657–3662.

Modesto-Lopez, L.B., & Biswas, P. (2010). Role of the effective electrical conductivity of nanosuspensions in the generation of $TiO_2$ agglomerates with electrospray. *Journal of Aerosol Science*, *41*, 790–804.

Norsworthy, G., Leidholm, C.R., Halani, A., Kapur, V.K., Roe, R., Basol, B.M., & Matson, R. (2000). CIS film growth by metallic ink coating and selenization. *Solar Energy Materials and Solar Cells*, *60*, 127–134.

Parretta, A., Addonizio, M., Loreti, S., Quercia, L., & Jayaraj, M. (1998). An investigation on the growth of thin chalcopyrite $CuInSe_2$ films by selenization of Cu–In alloys in a box. *Journal of Crystal Growth*, *183*, 196–204.

Romeo, A., Terheggen, M., Abou-Ras, D., Bätzner, D.L., Haug, F.J., Kälin, M., Rudmann, D., & Tiwari, A.N. (2004). Development of thin-film $Cu(In,Ga)Se_2$ and CdTe solar cells. *Progress in Photovoltaics: Research and Applications*, *12*, 93–111.

Roncallo, S., Painter, J., Cousins, M., Lane, D., & Rogers, K. (2008). A method to quantify the degree of uniformity of thickness of thin films. *Thin Solid Films*, *516*, 8493–8497.

Roncallo, S., Painter, J.D., Healy, M.J.F., Ritchie, S.A., Finnis, M.V., Rogers, K.D., Scragg, J.J., Dale, P.J., & Zoppi, G. (2011). Effects of different needles and substrates on $CuInS_2$ deposited by electrostatic spray deposition. *Thin Solid Films*, *519*, 3544–3551.

Sastry, D.V.K., & Reddy, P.J. (1983). Electrical conductivity, structure and hall effect measurements of InSe films. *Thin Solid Films*, *105*, 139–147.

Tomar, M., & Garcia, F. (1982). A ZnO/*p*-$CuInSe_2$ thin film solar cell prepared entirely by spray pyrolysis. *Thin Solid Films*, *90*, 419–423.

Yoon, H., Woo, J.H., Ra, Y.M., Yoon, S.S., Kim, H.Y., Ahn, S.J., Yun, J.H., Gwak, J., Yoon, K.H., & James, S.C. (2011). Electrostatic spray deposition of copper–indium thin films. *Aerosol Science and Technology*, *45*, 1448–1455.

Zhu, J., Koltypin, Y., & Gedanken, A. (1999). General sonochemical method for the preparation of nanophasic selenides: synthesis of ZnSe nanoparticles. *Chemistry of Materials*, *12*, 73–78.